Detection of Hepatocellular Carcinoma: Gadoxetic Acid–Enhanced 3-Dimensional Magnetic Resonance Imaging Versus Multi–Detector Row Computed Tomography

Young Kon Kim, MD, Chong Soo Kim, MD,* Young Min Han, MD,* Hyo Sung Kwak, MD,* Gong Yong Jin, MD,* Seung Bae Hwang, MD,* Gyung Ho Chung, MD,* Sang Yong Lee, MD,* and Hee Chul Yu, MD†*

Purpose: The aim of this study was to compare the diagnostic accuracy and sensitivity of gadoxetic acid–enhanced magnetic resonance imaging (MRI) with multi–detector row computed tomography (MDCT) for the detection of hepatocellular carcinomas (HCCs).

Materials: Sixty-two patients (81 HCCs) who underwent MDCT and gadoxetic acid–enhanced MRI using a 3-dimensional volumetric interpolated technique with a mean interval of 7 days (range, 3–11 days) were included in this study. Two observers reached a consensus on 2 sets of images: the gadoxetic acid set (unenhanced, early dynamic, 10-minute, and 20-minute hepatocyte phase images) and the 3-phase MDCT. Diagnostic accuracy and sensitivity were evaluated using the alternative-free response receiver operating characteristic method.

Results: There was a trend toward increased area under the receiver operating characteristic curve (Az value) for the gadoxetic acid set (0.963) as compared with the MDCT (0.930), but no significant difference was found ($P = 0.41$). Sensitivity of the gadoxetic acid set (91.4%) was better than that of the MDCT (71.6%; $P = 0.0001$). There were 12 lesions that showed only arterial hypervascularization on MDCT but showed arterial hypervascularization and delayed hypointensity on the gadoxetic acid set.

Conclusions: Gadoxetic acid–enhanced MRI, including hepatocyte phase imaging, is more sensitive than MDCT for the detection of HCCs.

Key Words: liver neoplasms, magnetic resonance (MR), contrast media, computed tomography (CT), technology

(*J Comput Assist Tomogr* 2009;33: 844–850)

Liver computed tomography (CT) and magnetic resonance imaging (MRI) using an extracellular space (ECS) contrast agent have played a central role in detecting and characterizing hepatocellular carcinoma (HCC).[1–4] With technical advances in liver imaging modalities and periodic follow-up examinations for those in the high-risk HCC group, atypical small HCCs that are seen as only arterially enhanced nodules are frequently encountered in clinical practice when using ECS agents.[5–9] When an ECS agent is used alone, this atypical appearance of HCCs is difficult to differentiate from nonneoplastic hypervascular pseudolesions, such as arterioportal shunts. Therein, many cases require an additional liver MRI using a liver-specific agent to accurately characterize these equivocal lesions.[5–9]

Gadolinium ethoxybenzyl diethylenetriaminepentaacetic acid (gadoxetic acid disodium) is a recently developed dual contrast agent that has combined properties of an ECS agent and a liver-specific agent.[10,11] Through many clinical trials, this agent has demonstrated satisfactory results in the detection and characterization of hepatic tumors, including HCC.[10–13] The most promising ability of this liver-specific agent may be the high sensitivity of its hepatocyte phase imaging to detect a small malignant liver tumor.[12,13] Taking into account the overlapping imaging findings of small HCCs and nonneoplastic hypervascular pseudolesions on dynamic CT or MRI when using an ECS agent, gadoxetic acid–enhanced liver MRI, including hepatocyte phase imaging, could be a promising tool, resolving the limitation of dynamic liver CT or MRI by increasing the accuracy of both HCC detection and characterization. To the best of our knowledge, there has been no study determining the diagnostic accuracy and sensitivity of gadoxetic acid–enhanced MRI for detecting HCC by comparing other liver imaging modalities in the same populations. Because multidetector CT is still the most commonly used imaging modality for HCC workup, we conducted this study to compare the diagnostic accuracies and sensitivities of gadoxetic acid–enhanced MRI and MDCT for the detection of HCC, using alternative-free response receiver operating characteristic (ROC) analysis.

MATERIALS AND METHODS

Patients

We retrospectively reviewed our institutional database for liver MRIs and CTs conducted on patients suspected of having HCC that were performed at our institution, a tertiary referral hospital, between June 2007 and August 2008. We identified 125 patients suspected of having HCC who underwent both a multiphase contrast-enhanced dynamic MDCT and a gadoxetic acid–enhanced liver MRI. Our hospital's institutional review board approved this retrospective study.

Of the 125 patients, only those patients that met the following criteria were included in the study. The criteria included (*a*) HCCs that had been proven based on histologic proof or image findings of diagnostic procedures including MDCT, MRI, hepatic angiography, and Lipiodol CT; (*b*) a time interval between MDCT and gadoxetic acid–enhanced MRI shorter than 15 days (range, 3–11 days; mean interval, 7 days); and (*c*) a follow-up contrast-enhanced CT or MRI performed at least 6 months later (range, 6–15 months). Furthermore, patients who had multinodular HCCs (more than 10) were excluded from this study because inclusion of these cases could

From the Departments of *Diagnostic Radiology, and †General Surgery, Medical School, Chonbuk National University Hospital, JeonJu, Republic of Korea.

Received for publication January 16, 2009; accepted March 30, 2009.

Reprints: Young Kon Kim, MD, Department of Diagnostic Radiology, Medical School, Chonbuk National University Hospital, Keum Am Dong, JeonJu, Republic of Korea (e-mail: jmyr@dreamwiz.com).

This study was supported by a grant (No. 0620220) from the National R&D Program for Cancer Control, Ministry of Health and Welfare, Republic of Korea.

heavily influence the statistical analysis of this study. Consequently, this study population included 62 patients (50 men and 12 women; age range, 40–74 years) with 81 HCCs (size range, 0.6–3.0 cm; mean, 1.5 cm). No study patients had liver masses other than the HCCs, regenerating nodules, and hepatic cysts. Fifty-six patients had liver cirrhosis or chronic hepatitis associated with viral hepatitis B, and 6 remaining patients had viral hepatitis C–induced liver cirrhosis. Based on the Child-Pugh classification,[14] 50 patients were classified as child class A; and the 5 remaining patients, as class B.

The final diagnosis for 23 patients (26 HCCs) was confirmed by the pathologic analysis of surgical specimens. Of these 26 HCCs, 22 lesions corresponded to grade I (n = 3) or II (n = 19) according to Edmondson's classification of HCC[15] and the remaining 4 lesions were grade III. For the 39 patients (55 HCCs) who underwent transarterial chemoembolization (n = 53) or radiofrequency ablation (n = 2), the reference standards were based on a consensual interpretation of matched findings for all diagnostic procedures by 2 experienced radiologists. The diagnostic procedures included the following: image-guided biopsy (n = 2), characteristic image findings on 3-phase MDCT and/or MRI (arterial hypervascularization and early washout, as well as arterial hypervascularization plus hyperintensity on superparamagnetic iron oxide–enhanced MRI),[16] persistent dense compact nodular Lipiodol uptake of the lesions detected only on MDCT and MRI,[17] and aggravation (local recurrence) seen at follow-up MDCT or MRI (n = 5).

Multi–Detector Row Computed Tomography

Computed tomography examinations were performed with an MDCT scanner (Sensation 16; Siemens, Forchheim, Germany) with 16 detector rows. Images were acquired throughout the liver in a craniocaudal direction with a 1.5 × 16-beam collimation. Other scanning parameters were as follows: 150 mAs, 120 kilovolts (peak) [kV(p)], a 1.5-mm detector collimation, a 24-mm per rotation table speed, a 3.0-mm reconstruction interval, and a 0.5-second gantry rotation time.

After acquisition of the unenhanced liver images, a contrast medium with a concentration of 370 mg of iodine per milliliter (Ultravist 370; Schering, Berlin, Germany) was administered using a power injector (multilevel CT; Medrad, Pittsburgh, Pa). The contrast medium was injected at a rate of 3 mL/s through an 18-gauge plastic intravenous catheter placed in an antecubital vein. The volume of contrast medium delivered varied depending on the body weight of each patient (2 mL/kg of body weight); therefore, the total volume of contrast medium administered was 110 to 150 mL (mean [SD], 120 [10] mL). Determination of the scanning delay for arterial phase imaging was achieved using an automatic bolus tracking technique (Siemens). The single-level monitoring low-dose scanning (120 kV[p], 20 mA) was initiated 10 seconds after contrast injection. The contrast enhancement was automatically calculated in the ROI cursor placed over the vessel of interest (abdominal aorta), and the level of the trigger threshold was set at an increase of 80 Hounsfield units. Fifteen seconds after the trigger threshold was reached, the arterial phase scanning began automatically.[18] The mean scanning delay for dynamic 3-phase images, including the arterial, portal, and equilibrium phases, were 38, 70, and 180 seconds, respectively, after the start of contrast media injection.

Magnetic Resonance Examination

All MRIs were performed using a 1.5-T superconducting imager (Magnetom Symphony; Siemens, Erlangen, Germany) with a combination of a phased-array body coil and a spine-array coil for signal reception.

A transverse volumetric 3-dimensional fat-suppressed spoiled gradient-echo acquisition (volumetric interpolated breath-hold examination; Siemens) with mSENSE was performed using the following parameters: a repetition time–echo time of 4.3:2.0, a 12-degree flip angle, a 450-Hz/pixel bandwidth, a matrix of 256 (read) × 135 (phase) × 40 to 46 (partition), a 2.5- to 3.0-mm effective slice thickness, and a field of view of 32 to 35 cm. After the unenhanced images were acquired, all patients received a dose of 0.025 mmol/kg of body weight of 0.25-mol/L gadoxetic acid disodium solution (volume range, 8–10 mL), administered intravenously at a rate of 2 mL/s, and followed by a 20-mL saline flush. Time for the dynamic arterial phase imaging was achieved using the MR fluoroscopic bolus detection technique (CARE Bolus; Siemens). The mean delay times (the time interval between bolus administration and the start of image acquisition) for the arterial, portal, and equilibrium phases were 30, 60, and 180 seconds, respectively. Then, 5 minutes after the injection of the contrast media, a fat-suppressed, respiratory-triggered, T2-weighted, turbo spin-echo sequence was obtained using the following parameters: repetition time–echo time of 3378:71 to 4620:71, an echo train length of 13, a 150-degree flip angle, a matrix of 144 × 256, a 6-mm slice thickness, a chemically selective fat suppression, and a mean scan time of 3 minutes for 20 slices. Finally, a hepatocyte-specific phase image was acquired 10 and 20 minutes after contrast media was administered.

Imaging Analysis

Image analysis was performed by 2 faculty-level gastrointestinal radiologists with experience interpreting liver CT and MRI during their daily clinical practice. All of the acquired images were reviewed on a 2000 × 2000 picture archiving and communication systems monitor (Marotech, Seoul, South Korea). The 2 radiologists were unaware of the results of all of the other image findings and the final diagnosis. Two separate sets of images were analyzed in random order, including the MDCT and the gadoxetic acid set (precontrast, arterial, portal, 3-minute delay, and 10- and 20 minute hepatocyte phases of 3-dimensional MR images plus T2-weighted images [T2WI]). To minimize any learning bias, there was a 3-week interval between the blinded interpretations. Because we were not interested in evaluating the absolute detecting sensitivity of the 2 different imaging modalities and wanted to find the discordance features of HCC between MDCT and MRI, a consensus between the 2 reviewers was acquired during image analysis. However, to determine the reproducibility for the diagnostic capability of the gadoxetic acid set, 2 observers independently evaluated the MR images at the first reading session and then jointly evaluated the results until a consensus was reached. Disagreements were minimal and were easily resolved.

The observers recorded the presence and location of the lesions, assigning each lesion a confidence level based on a 4-point scale. The lesions were scored as follows: 0, not visible; 1, lesions that showed only arterial hypervascularization with no delayed capsular enhancement,[19] washout, or T2 hyperintensity (category 4); 2, lesions that showed arterial hypervascularization with suspicious delayed capsular enhancement; 3 for lesions that showed arterial hypervascularization with definitive capsular rim on portal and/or equilibrium phase or suspicious delayed washout; and 4, lesions that showed arterial hypervascularization with definitive delayed washout (including hypointensity on gadoxetic acid–enhanced hepatocyte phase images) and/or

TABLE 1. Distribution of 81 HCCs According to MDCT and MRI Grade

	MRI Grade				
CT Grade	**0**	**1**	**2**	**3**	**4**
0	0	1	0	1	1
1	0	2	0	5	11
2	0	0	0	1	1
3	0	2	0	1	10
4	0	1	1	1	42

hyperintensity on T2WI. In addition, for the lesions that were seen as hypointense (hypoattenuated) during the early dynamic CT and MRI or at the 10- and 20-minute hepatocyte phase MRIs, the lesions were regarded as category 1 if they did not accompany hyperintensity on T2WIs.

Statistical Analysis

Based on the reviews submitted by the 2 observers, alternative-free response ROC curve analysis was performed on a lesion-by-lesion basis.[20] For each imaging set, an alternative-free response ROC curve was fitted to the confidence rating data using a maximum likelihood estimation program (Rockit 0.9B; courtesy of C.E. Metz, University of Chicago, Chicago, Ill, 1998).[21] The diagnostic accuracy of each imaging set and observer was assessed by calculating the area under the alternative-free response ROC curve (Az). The differences between the imaging sets, approximately the mean area under the alternative-free response ROC curves, were statistically analyzed using the 2-tailed Student *t* test for paired data. The sensitivities of each of the image sets were then calculated. The sensitivity for each set of images was evaluated according to the number of lesions assigned a confidence level of 3 or 4 among the 81 lesions. The sensitivities of both image sets were then compared using the McNemar test. A 2-tailed $P < 0.05$ was considered a significant difference. To provide a range of plausible sensitivity differences, we also calculated the 95% confidence intervals (CIs).[22]

To assess interobserver agreement for the evaluation of the gadoxetic acid set, we calculated the κ statistic for multiple observers.[23] Agreement between the blinded observers is reported later in κ values, with κ values greater than 0 indicating positive correlations; less than 0.20, positive but poor agreement; 0.21 to 0.40, fair agreement; 0.41 to 0.60, moderate agreement; 0.61 to 0.80, good agreement; and greater than 0.81, excellent agreement. All statistical analyses were calculated with SPSS 8.0 software (SPSS, Chicago, Ill).

RESULTS

Of the 67 patients, 59 had solitary lesions, 4 had 2 lesions, 3 had 3 lesions, and 1 had a total of 5 lesions. Of 81 lesions, 67 were 20 mm or less in diameter, and the remaining 14 lesions ranged from 21 to 30 mm in diameter. Table 1 shows the distributions of 81 HCCs according to confidence levels of MDCT and MRI for HCC detection. For the gadoxetic acid set, the Az values for individual reviewing were 0.975 for observer 1 and 0.964 for observer 2. For the consensus reading of the 2 observers, the Az value of the gadoxetic acid set (Az, 0.963) was slightly higher than the Az value of the MDCT (Az, 0.930), but no statistically significant difference of the Az values between both image sets was reached ($P = 0.410$). Among the 81 HCCs, the gadoxetic acid set allowed for the depiction of 74 lesions (sensitivity, 91.4%; 95% CI, 83.0-96.4%) as discerned by observer 1 and 72 lesions (sensitivity, 88.9%; 95% CI, 79.9–94.8%) as discerned by observer 2. The MDCT allowed for the depiction of 58 lesions (sensitivity, 71.6%; 95% CI,

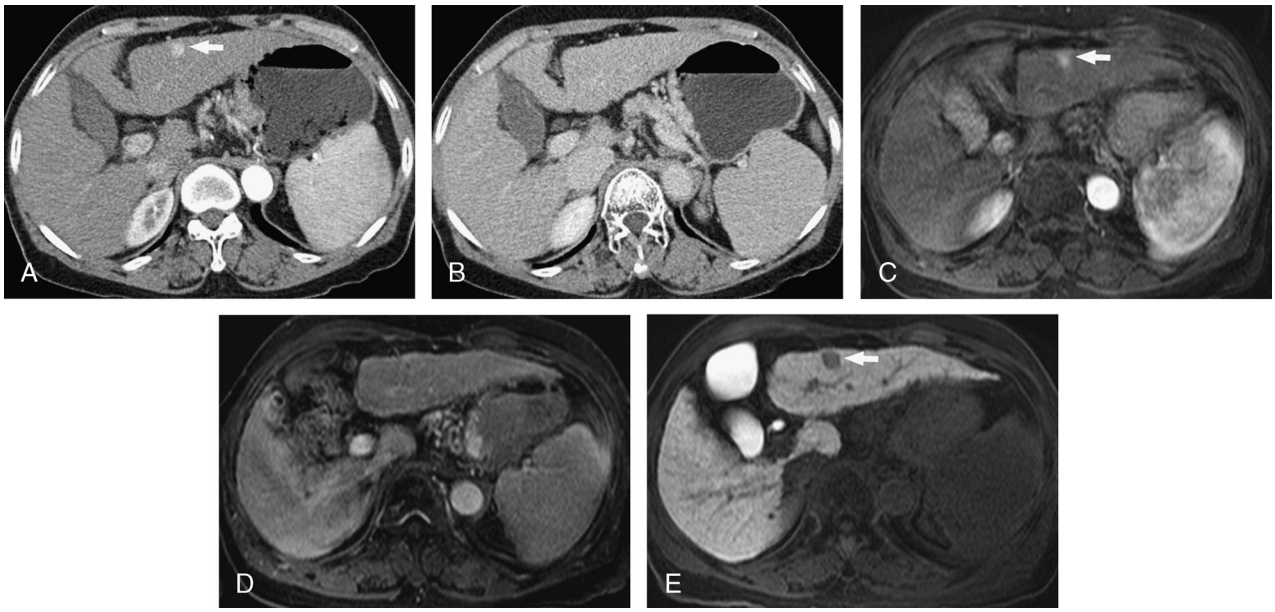

FIGURE 1. A 55-year-old man with 1.0-cm HCC. A, Arterial phase image of MDCT scanning showing a nodular enhancement in liver segment 3 (arrow). B, Equilibrium phase image of MDCT scanning showing no visible mass. C, Arterial-phase 3-dimensional MR image after the administration of gadoxetic acid (4.3/2.0) showing a nodular enhancement at the same location as in A (arrow). D, Three-minute late-phase 3-dimensional MR image after administration of gadoxetic acid (4.3/2.0) showing no visible mass. E, Axial gadoxetic acid–enhanced 20-minute hepatocyte phase image (4.3/2.0) clearly showing a hypointense mass (arrow).

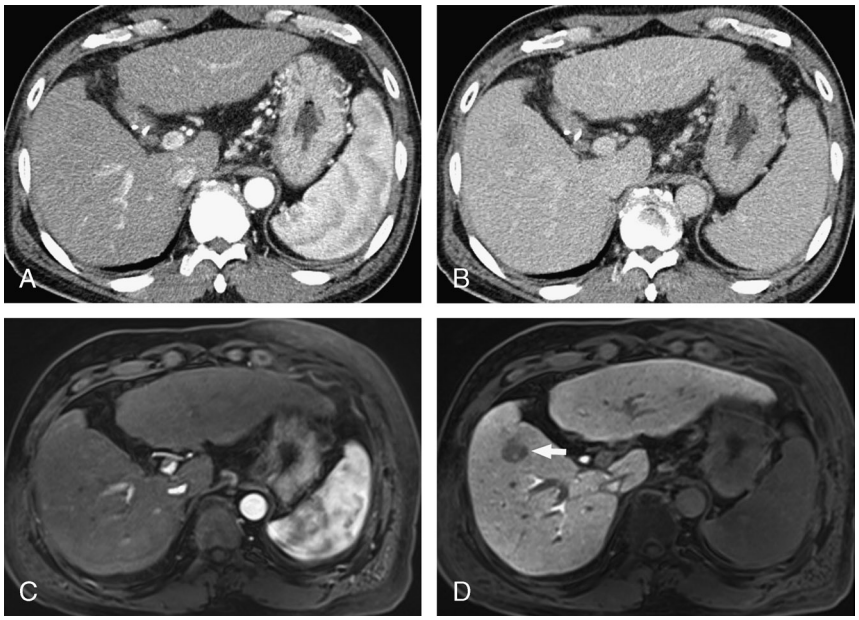

FIGURE 2. Well-differentiated hypovascular HCC in a 62-year-old man. A, Arterial phase image of MDCT scanning showing no visible mass. B, Equilibrium phase image of MDCT scanning showing no visible mass. C, Arterial phase 3-dimensional MR image after the administration of gadoxetic acid (4.3/2.0) showing no visible mass. D, Gadoxetic acid–enhanced 20-minute hepatocyte phase image (4.3/2.0) clearly showing a hypointense mass (arrow).

60.5–81.1%). Thus, the sensitivity of the gadoxetic acid set for a consensus reading (sensitivity, 91.4%; 95% CI, 83.0–96.4%) was significantly higher than that of the MDCT (P = 0.0001; Fig. 1).

There were 3 HCCs (0.8, 1.0, and 1.2 cm) that could not be verified with both MRI and MDCT. During the retrospective review of these lesions, 2 lesions were seen as enhancing hyperintense nodules during the arterial phase imaging of MDCT and MRI but were occult at other images including portal and equilibrium phase imaging, as well as hepatocyte phase MRI. The remaining 1 lesion (1.2 cm) was clearly depicted as hypointense only at 10- and 20-minute hepatocyte phases of gadoxetic acid–enhanced MRI, which proved to be a well-differentiated HCC (Fig. 2). There were 20 lesions (0.3–1.5 cm)

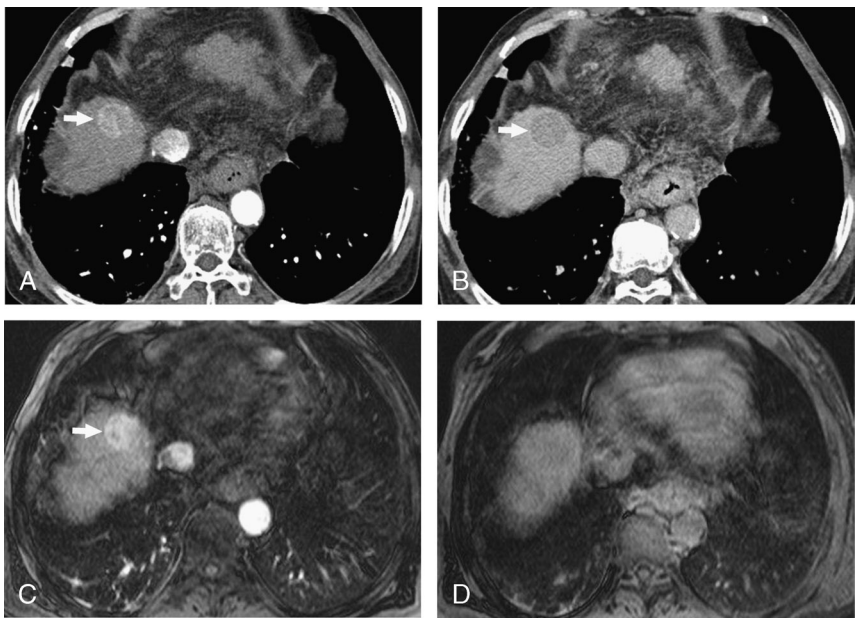

FIGURE 3. Nodular HCC in a 61-year-old man. A, Arterial phase image of MDCT scanning showing a nodular enhancing mass in the hepatic dome (arrow). B, Equilibrium phase image of MDCT scanning showing definitive washout of the mass (arrow). C, Arterial-phase 3-dimensional MR image after the administration of gadoxetic acid (4.3/2.0) showing a nodular enhancing mass at the same location as in A (arrow). D, Axial gadoxetic acid–enhanced 20-minute hepatocyte phase image (4.3/2.0) showing no visible mass.

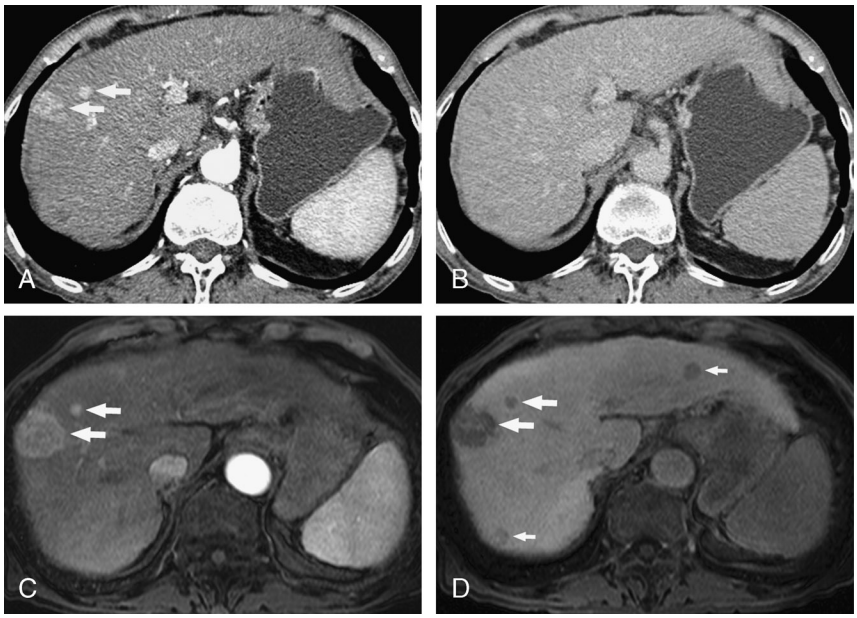

FIGURE 4. A 58-year-old man with multinodular HCCs. A, Arterial phase image of MDCT scanning showing nodular enhancing masses (arrows). B, Equilibrium phase image of MDCT scanning showing no definitive washout of the masses. C, Arterial phase 3-dimensional MR image after the administration of gadoxetic acid (4.3/2.0) showing a nodular enhancing mass and adjacent tiny daughter nodule at the same location as in A (arrows). D, Axial gadoxetic acid–enhanced 20-minute hepatocyte phase image (4.3/2.0) showing definitive washout of the masses (arrows). Note additional small hypointense nodules (small arrows), which were assigned a confidence level of 1 and proved to be cirrhosis-related benign nodules.

in 17 patients that were not detected on the MDCT but were clearly revealed on the gadoxetic acid set with a confidence rating of 3 or 4. Of these 20 lesions, 2 lesions were not depicted at all on 3-phase MDCT and were thereby rated with a confidence level of 0. Eighteen of the lesions showed only arterial hypervascularization with no definitive delayed capsular rim or washout at MDCT (confidence level, 1 or 2), but most of them showed definitive washout on 3-minute late phase MRI (n = 9) and/or hypointensity at 10- and 20-minute hepatocyte phase MRIs (n = 12; Fig. 1). There was no lesion that was detected only on the portal and/or 3-minute late phase images of gadoxetic acid–enhanced MRI but not on the 10- and 20-minute hepatocyte phase images. There was no difference in liver lesion detectability between the 10-minute hepatocyte phase MRI and the 20-minute hepatocyte phase MRI.

To the contrary, there were 4 lesions that were detected only on the MDCT but were not verifiable on the gadoxetic acid set (Fig. 3). They were shown as hypervascular nodules on gadoxetic acid–enhanced arterial phase imaging but were not depicted or showed isointensity on 3-minute late phase or hepatocyte phase imaging and on T2WI (confidence rating of 1 or 2). Two of them proved to be grades I and II according to Edmondson's classification of HCC. However, there was no HCC that was assigned a confidence rating of 0 with MRI but was detected on the MDCT. For both image sets, there were no false-positive findings with a confidence rating of 3 or 4. However, there were 3 hypointense nodules (0.6–0.8 cm) that were shown only with the hepatocyte phase imaging of gadoxetic acid–enhanced MRI, which were assigned a confidence rating of 1 (Fig. 4). These nodules proved to be cirrhosis-related benign nodules (regenerative or dysplastic nodules) because no evidence of HCC was seen using other imaging modalities at follow-up or in the biopsy specimen.

The κ value for the 2 observers was 0.816 for the gadoxetic acid set, indicating good interobserver agreement on the presence of lesions.

DISCUSSION

Considering the high potency of gadoxetic acid–enhanced hepatocyte phase imaging in the detection of liver malignancy, we hypothesized that gadoxetic acid–enhanced MRI would be more sensitive than MDCT in detecting HCC by increasing the delineation of HCC on the hepatocyte phase imaging. However, although many clinical trials have shown that gadoxetic acid offers hemodynamic information for lesion characterization during early vascular-interstitial distribution comparable to the conventional gadolinium chelates,[10,11] a major concern in using gadoxetic acid for HCC workup is if the ability of gadoxetic acid to show arterial hypervascularization of HCC is comparable to other ECS agents, especially in detecting small HCC. This is because commercially available gadoxetic acid dose at present is less than half of that of other conventional gadolinium-based ECS agents.[10–12] Therefore, through this study, we wanted to evaluate the diagnostic capability of gadoxetic acid in detecting HCC by comparing MDCT in its ability to show the arterial hypervascularization of HCC during the arterial phase and to delineate washout of HCC or the additional delineation of HCC with hepatocyte phase MRI.

When our study cases were retrospectively reviewed, there were no cases of HCC that were seen only as a hypervascular nodule on the MDCT but showed no hypervascularization on the gadoxetic acid–enhanced arterial phase imaging. On the contrary, there were 2 lesions that were seen as typical hypervascular HCCs on the gadoxetic acid–enhanced MRI but were not depicted on 3-phase MDCT. Given that the mean delay time after the administration of contrast media for the arterial phase of MDCT in our study did not differ from the ideal timing reported

for arterial phase imaging by the previous studies,[24,25] this phenomenon could be explained by the inherent higher soft tissue contrast of MRI relative to CT and higher T1 relaxivity in human plasma of gadoxetic acid (8.7 L $mmol^{-1}$ s^{-1} in H_2O at 0.47 T) compared with an ECS agent such as gadopentetate dimeglumine (4.1 L $mmol^{-1}$ s^{-1}; Magnevist; Schering),[26] although the gadoxetic acid dose is lower than other conventional gadolinium-based agents. Therefore, given that MDCT has shown comparable capabilities for detecting HCC to gadolinium-based MRI,[27,28] our study result could indicate that the ability of gadoxetic acid to delineate arterial hypervascularization of HCC is comparable to other ECS MR contrast agents.

This study revealed that in alternative free response ROC analysis, there was a trend toward increased diagnostic accuracy (Az) with gadoxetic acid–enhanced MRI (Az, 0.963) than with MDCT (Az, 0.930), but a statistically significant difference was not reached ($P = 0.41$). However, the sensitivity for detecting HCC with gadoxetic acid–enhanced MRI was significantly higher than that with MDCT ($P = 0.0001$). There were 12 lesions that showed only arterial hypervascularization with no definitive delayed peripheral rim and washout on MDCT but showed arterial hypervascularization and washout on a 3-minute late phase MRI and/or hypointensity at a 10- and 20-minute hepatocyte phase MRIs. Thus, the main contributing factor for higher sensitivity of gadoxetic acid MRI than MDCT in this study could be the difference in the ability of 2 imaging modalities to delineate the washout of hypervascular HCC. This means that gadoxetic acid MRI is superior to MDCT in accurately characterizing nodular enhancements detected on arterial phase imaging. The sensitivity of MDCT in this study was relatively lower in comparison to other study results.[27–29] This might be attributed to the fact that most study cases consisted of small nodular HCCs that are less than 2 cm; because small HCCs tend to manifest only as an arterially enhanced lesion on dynamic CT, this does not fit the definitive diagnostic criteria for HCC.[5–9] Furthermore, to avoid introducing bias during an individual reviewing session, we made a strict guideline for confidence levels beforehand, so most of the lesions that were depicted only at arterial phase imaging as hyperintense were considered "not HCC (rating scale 1)," regardless of the subjective decision of each reviewer.

In the contrary, there were 4 lesions that showed arterial hypervascularization and rapid washout or delayed capsular rim on the MDCT but were not verifiable on the gadoxetic acid set. On gadoxetic acid–enhanced 3-minute late or 10- and 20-minute hepatocyte phase imagings, they were seen as isointense because of the uptake of contrast media, which may be more frequent in cases of a well-differentiated HCC.[11] This could be one shortcoming of using gadoxetic acid in an HCC workup because, as for the isointense or hyperintense nodules at hepatocyte phase imaging that are resulted from their contrast uptake, there has been no exact guideline for differentiating between HCC and cirrhosis-related benign nodules, except when they show T2 hyperintensity.

We found 4 hypointense nodules that were depicted only at gadoxetic acid–enhanced hepatocyte phase imaging as rating score 1. Three of them were considered to be cirrhosis-related benign nodules because they showed no evidence of malignancy by other imaging modalities or other MR sequence and biopsy specimens. In our clinical experiences, we have frequently encountered small hypointense nodules that are depicted only by gadoxetic acid–enhanced hepatocyte phase imaging. If they do not accompany arterial hypervascularization or T2 hyperintensity, they could not be regarded as definitive HCCs. However, the one remaining nodule that was depicted only by hepatocyte phase MRI proved to be well-differentiated HCC (Fig. 2). Therefore, the delineation of these lesions only by gadoxetic acid–enhanced hepatocyte phase image alone could have a positive or negative impact on the treatment plan. However, given that the HCC risk group generally has periodic screenings, early recognition of these risky hepatic nodules with malignant potential could lead to the early detection of HCC by encouraging patients with these hepatic nodules to undergo a more careful follow-up. For a clear definition and classification of these nodular lesions, further evaluation of a large number of pathologically proven cases will be warranted.

Several limitations of this study should be noted. First, not all of the lesions were confirmed surgically, which may have resulted in some degree of overestimation of the actual sensitivity of both image modalities by reducing the number of false-negative lesions. The objective of our study, however, was not to determine the absolute diagnostic accuracy and sensitivity of liver imaging modalities about detection but to compare the diagnostic accuracy and sensitivity between the 2 different imaging modalities. We assume that the most precise determination of the total number of lesions is possible only through liver transplantation and matched-pair analysis performed to verify that the lesions detected on MRI correspond to the lesions in the resected liver specimen. However, even though we had pathologic specimens for all lesions detected by MRI, controversy still exists based on the pathologic diagnosis when differentiating equivocal lesions, such as hypointense nodules detected only by hepatocyte phase MRI, as being dysplastic nodules or well-differentiated HCCs. Second, the Az values and sensitivity of MDCT and MRI were acquired based on the consensus between 2 observers to avoid introducing individual bias into the statistical results because the signal intensities of HCCs and cirrhosis-related benign nodules on gadoxetic acid–enhanced hepatocyte phase imaging have not yet been determined. Through this approach, we could determine the differential imaging features of HCC between 3 phasic MDCT and gadoxetic acid–enhanced MRI. Furthermore, although we used an alternative-free response ROC analysis for lesion detection, as for the inherent methodological limitations, an assessment regarding lesion characterization was inevitably taken into account during the image analysis for lesion detection. Third, because we did not include compartmental modeling of the contrast agent pharmacokinetics and the key kinetic partition coefficients were undetermined, we could not exactly establish the start of the hepatocyte phase and optimal timing for the equilibrium phase of gadoxetic acid–enhanced MRI. Therefore, we could not determine whether the hypointensity of HCC on the 3-minute late phase image resulted from the washout of HCC or the pure efficacy of hepatocyte phase imaging to delineate hepatic malignancy.

In conclusion, for the detection of HCCs, the gadoxetic acid–enhanced 3-dimensional liver MRI showed better sensitivity than the MDCT by means of increasing the delineation of hypointensity of HCC at 3-minute late phase and hepatocyte phase imagings.

REFERENCES

1. Kim T, Murakami T, Oi H, et al. Detection of hypervascular hepatocellular carcinoma by dynamic MRI and dynamic spiral CT. *J Comput Assist Tomogr*. 1995;19:948–954.
2. Van Leeuwen MS, Noordzij J, Feldberg MA, et al. Focal liver lesions: characterization with triphasic spiral CT. *Radiology*. 1996;201: 327–336.

3. Kwak HS, Lee JM, Kim CS. Preoperative detection of hepatocellular carcinoma: comparison of combined contrast-enhanced MR imaging and combined CT during arterial portography and CT hepatic arteriography. *Eur Radiol*. 2004;14:447–457.
4. Hamm B, Thoeni RF, Gould RG, et al. Focal liver lesions: characterization with nonenhanced and dynamic contrast-material-enhanced MR imaging. *Radiology*. 1994;190: 417–423.
5. Jeong YY, Mitchell DG, Kamishima T. Small (<20 mm) enhancing hepatic nodules seen on arterial phase MR imaging of the cirrhotic liver: clinical implications. *AJR Am J Roentgenol*. 2002;178:1327–1334.
6. Kanematsu M, Kondo H, Semelka RC, et al. Early-enhancing non-neoplastic lesions on gadolinium-enhanced MRI of the liver. *Clin Radiol*. 2003;58:778–786.
7. Shimizu A, Ito K, Koike S, et al. Hepatic enhancement in multiphasic contrast-enhanced MDCT: comparison of high- and low-iodine-concentration contrast medium in same patients with chronic liver disease. *AJR Am J Roentgenol*. 2004;183:157–162.
8. Holland AE, Hecht EM, Hahn WY, et al. Importance of small (< or = 20-mm) enhancing lesions seen only during the hepatic arterial phase at MR imaging of the cirrhotic liver: evaluation and comparison with whole explanted liver. *Radiology*. 2005;237:938–944.
9. Kim YK, Lee YH, Kim CS, et al. Added diagnostic value of T2-weighted MR imaging to gadolinium-enhanced three-dimensional dynamic MR imaging for the detection of small hepatocellular carcinomas. *Eur J Radiol*. 2008;67:304–310.
10. Halavaara J, Breuer J, Ayuso C, et al. Liver tumor characterization: comparison between liver-specific gadoxetic acid disodium-enhanced MRI and biphasic CT—a multicenter trial. *J Comput Assist Tomogr*. 2006;30:345–354.
11. Huppertz A, Haraida S, Kraus A, et al. Enhancement of focal liver lesions at gadoxetic acid–enhanced MR imaging: correlation with histopathologic findings and spiral CT—initial observations. *Radiology*. 2005;234:468–478.
12. Huppertz A, Balzer T, Blakeborough A, et al. Improved detection of focal liver lesions at MR imaging: multicenter comparison of gadoxetic acid–enhanced MR images with intraoperative findings. *Radiology*. 2004;230:266–275.
13. Kim YK, Lee YH, Kwak HS, et al. Detection of liver metastases: gadoxetic acid–enhanced three-dimensional MR imaging versus ferucarbotran-enhanced MR imaging. *Eur J Radiol*. 2009. In press.
14. Pugh RN, Murray-Lyon IM, Dawson JL, et al. Transection of the esophagus for bleeding esophageal varices. *Br J Surg*. 1973;60: 646–649.
15. Edmondson HA, Steiner PE. Primary carcinoma of liver: study of 100 cases among 48,900 necropsies. *Cancer*. 1954;7:462–503.
16. Kim YK, Kwak HS, Han YM, et al. Usefulness of combining sequentially acquired gadobenate dimeglumine–enhanced magnetic resonance imaging and resovist-enhanced magnetic resonance imaging for the detection of hepatocellular carcinoma: comparison with computed tomography hepatic arteriography and computed tomography arterioportography using 16-slice multidetector computed tomography. *J Comput Assist Tomogr*. 2007;31:702–711.
17. Lencioni R, Pinto F, Armillotta N, et al. Intrahepatic metastatic nodules of hepatocellular carcinoma detected at Lipiodol CT: imaging-pathologic correlation. *Abdom Imaging*. 1997;22:253–258.
18. Kim MJ, Choi JY, Lim JS, et al. Optimal scan window for detection of hypervascular hepatocellular carcinomas during MDCT examination. *AJR Am J Roentgenol*. 2006;187:198–206.
19. Grazioli L, Ollivetti L, Fugazzola C, et al. The pseudo-capsule in hepatocellular carcinoma: correlation between dynamic MR imaging and pathology. *Eur Radiol*. 1999;9:62–67.
20. Chakraborty DP, Winter LH. Free-response methodology: alternate analysis and a new observer-performance experiment. *Radiology*. 1990;74:873–881.
21. Metz CE. ROC methodology in radiologic imaging. *Invest Radiol*. 1986;21:720–733.
22. Rao JN, Scott AJ. A simple method for the analysis of clustered binary data. *Biometrics*. 1992;48:577–585.
23. Landis JR, Koch GG. The measurement of observer agreement for categorical data. *Biometrics*. 1977;33:159–174.
24. Lee KH, Choi BI, Han JK, et al. Nodular hepatocellular carcinoma: variation of tumor conspicuity on single-level dynamic scan and optimization of fixed delay times for two-phase helical CT. *J Comput Assist Tomogr*. 2000;24:212–218.
25. Francis IR, Cohan RH, McNulty NJ, et al. Multidetector CT of the liver and hepatic neoplasms: effect of multiphasic imaging on tumor conspicuity and vascular enhancement. *AJR Am J Roentgenol*. 2003;180:1217–1224.
26. Schuhmann-Giampieri G, Schmitt-Willich H, Press WR, et al. Preclinical evaluation of Gd-EOB-DTPA as a contrast agent in MR imaging of the hepatobiliary system. *Radiology*. 1992;183:59–64.
27. Kim YK, Kim CS, Chung GH, et al. Comparison of gadobenate dimeglumine-enhanced dynamic MRI and 16-MDCT for the detection of hepatocellular carcinoma. *AJR Am J Roentgenol*. 2006;186:149–157.
28. Noguchi Y, Murakami T, Kim T, et al. Detection of hypervascular hepatocellular carcinoma by dynamic magnetic resonance imaging with double-echo chemical shift in-phase and opposed-phase gradient echo technique: comparison with dynamic helical computed tomography imaging with double arterial phase. *J Comput Assist Tomogr*. 2002;26:981–987.
29. Kim SJ, Kim SH, Lee J, et al. Ferucarbotran-enhanced 3.0-T magnetic resonance imaging using parallel imaging technique compared with triple-phase multidetector row computed tomography for the preoperative detection of hepatocellular carcinoma. *J Comput Assist Tomogr*. 2008;32:379–385.